

A Tilted Dark Halo Origin of the Galactic Disk Warp and Flare

Jiwon Jesse Han, Charlie Conroy, and Lars Hernquist
Center for Astrophysics | Harvard & Smithsonian, Cambridge, MA, USA

The outer disk of the Milky Way Galaxy is warped and flared. Several mechanisms have been proposed to explain these phenomena, but none have quantitatively reproduced both features. Recent work has demonstrated that the Galactic stellar halo is tilted with respect to the disk plane, suggesting that at least some component of the dark matter halo may also be tilted. Here we show that a dark halo tilted in the same direction as the stellar halo can induce a warp and flare in the Galactic disk at the same amplitude and orientation as the data. In our model the warp is visible in both the gas and stars of all ages, which is consistent with the breadth of observational tracers of the warp. These results, in combination with data in the stellar halo, provide compelling evidence that our Galaxy is embedded in a tilted dark matter halo. This misalignment of the dark halo and the disk holds clue to the formation history of the Galaxy, and represents the next step in the dynamical modeling of the Galactic potential.

We construct a model of the gravitational potential of the Galaxy in which 30% of the dark halo mass is comprised of a triaxial distribution that is tilted 25° with respect to the disk plane. The potential also includes bulge and disk components, where the latter increases in time to mimic the growth of the Galactic disk with time. We calculate the orbits of collisionless (stars) and collisional (gas) particles over 5 Gyr in this potential. In Figure 1 we show the present-day distribution of stars in the simulation. In the top panel we plot the Galactocentric vertical height (Z) and signed cylindrical radius (R), clearly revealing an S-shaped *warp* of the disk. Negative R indicates the Galactic quadrants that are within $\pm 90^\circ$ of the positive peak (the “Northern” warp) and positive R indicates Galactic quadrants that are within $\pm 90^\circ$ of the negative peak (the “Southern” warp). In the bottom panels, we plot the vertical deviation ($Z - Z_{\text{warp}}$) of tracer particles from the mean warp. The average vertical deviation grows markedly towards outer radii, demonstrating the *flare* of the disk. Particles are color-coded by age, which shows that stars of all ages exhibit a warp and flare. The warp is most pronounced for the youngest stars, consistent with observations^{1,2}.

In Figure 2 we compare the warp and flare of the simulated stars (left panel) and gas (right panel) to observations. For conciseness of comparison, we focus on the HI^{3,4} gas and Cepheid¹ stars. We note that a similar warp has also been ob-

served for ionized gas⁵, molecular gas⁶, dust⁷, stars^{2,8–10}, and star clusters¹¹. In the top panels we plot the observed warp in open circles, and a maximum likelihood fit to the simulation in solid colored lines, with 1σ uncertainty of the fit shaded. The onset radius R_w of the fit is fixed to the observed R_w values. The flare is measured by fitting an exponential scale height to the vertical deviation from the warp at each radius. In both stars and gas, the simulated warp and flare quantitatively match the observations. Additionally, the tilted halo simulation produces a population of stars on circular orbits that reach high-latitude ($|Z| > 2$ kpc) on either side of the warp extrema. This population of stars is reminiscent of known stellar overdensities towards the Galactic anticenter^{10,12–14}.

The parameters chosen for the simulation were not tuned to match the Galactic warp or flare. The two key parameters affected the predicted warp and flare are: (1) the shape and extent of the tilted halo, and (2) the scale radius of newly-formed stars. For the former, we adopt the scale radius, triaxiality, and tilt angle of the halo directly from the shape of the accreted stellar halo¹⁵. For the latter, we adopt the scale radius of the molecular disk of the Galaxy¹⁶. Details of the simulation setup and variations to the adopted parameters are given in the Supplementary Material.

The large-scale warp of the Galactic disk has been known for over half a century^{17,18}, and there is a commensurately rich history of warp and flare models^{19–22}. For example, studies have investigated the warp as a result of perturbed bending modes²³, misaligned angular momenta of the halo and the disk^{24,25}, repeated impact from the Sagittarius dwarf galaxy²⁶, misaligned gas accretion²⁷, or quadrupolar torque from a tumbling triaxial halo²⁸. However, previous studies have been unable to quantitatively reproduce the warp (and simultaneously the flare) of the Galactic disk. Among the recently investigated models is the tidal influence of the Large Magellanic Cloud (LMC)²⁹. In Figure 3 we plot the disk warp at $R = 16$ kpc produced by the tilted halo model and an LMC model as a function of Galactic longitude. The LMC was modeled as a live halo on its first infall into a live Milky Way halo and disk²⁹. The HI data³ at this radius is marked in open circles. Even for the highest LMC mass—which is 80% higher than other models³⁰—the warp amplitude is less than a third of the observed amplitude. In the right panel, we sum the amplitudes of the warp from the LMC and the tilted halo models. The combined model matches the observa-

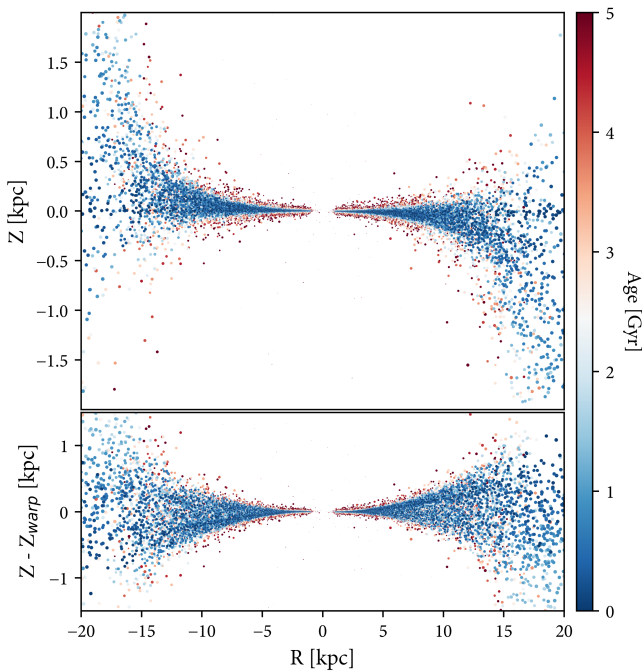


Figure 1: Present-day distribution of simulated stars in Galactocentric cylindrical coordinates. Negative R indicates azimuthal angles that are within 90° of the Northern warp, and positive R indicates azimuthal angles that are within 90° of the Southern warp. The top panels show the warp, and the bottom panels show the vertical deviation from the average warp. The vertical deviation systematically increases toward the outer Galaxy, demonstrating the flare of the disk. Points that are in the outer Galaxy are plotted with larger markers. Particles colored by stellar age clearly demonstrate a warp at all ages, and most strongly at the youngest population.

tions better than the tilted halo alone, although we caution that this simple summation does not capture the possible coupling between the effect of the LMC and the tilted halo.

Tilted dark halos are common in galaxy simulations that include baryonic physics^{31,32}, and several independent lines of evidence have pointed toward a tilted Galactic dark halo^{33–35}. Furthermore, Han et al. (in prep) show that such tilted dark halos are long-lived and can warp Galactic disks in Illustris TNG50^{36,37}. In a realistic model we can expect the tilt angle to change with time, for example due to interaction between the (growing) disk and the halo. While the tilt of the halo at earlier epochs can leave interesting observational signatures in old disk stars, the main point of this paper is to demonstrate that the young disk (and gas) is responsive to the tilt on < 1 Gyr timescales, and on such timescales the tilt is constrained observationally to be $\sim 25^\circ$. A plausible origin of a tilted dark halo in the Galaxy is a major merger^{38,39} 8 – 10 Gyr ago^{40,41} that deposited a significant fraction of dark matter on an eccentric, tilted orbit^{35,42}. Dynamical models of the Galaxy often assume a spherical dark halo at all scales, or a flattened halo that is aligned with the disk. A tilted dark halo at ~ 30 kpc would have novel applications for Galactic dynamics. For example, a tilted and

triaxial halo influences the shape of the stellar halo³⁵, and can affect orbit reconstruction of stellar streams⁴³. Furthermore, the tilt and triaxiality of the inner halo ($\sim 0.1R_{\text{virial}}$) encodes information about the self-interacting properties of dark matter⁴⁴ that is unique compared to larger-scale probes such as galaxy clusters or large scale structure. Future work will investigate the imprint of dark matter self-interaction through the tilt and triaxiality of the dark halo at 30 kpc. In addition, a global tilt in the dark halo implies an anisotropic velocity distribution of the dark matter particles. The resulting asymmetric velocity distribution should affect ground-based dark matter detection experiments⁴⁵.

Finally, while we have focused on demonstrating that the warp and flare are likely manifestations of a tilted dark halo, we can also reverse the argument: precise measurements of the warp may further constrain the tilt of the dark halo. We have intentionally avoided “fitting” a dark halo to match the warp, but there is much to explore in allowing for more flexible halo models. For example, the warp is sensitive to the tilt angle of the dark halo, and the fraction of mass in the tilted component (see Methods). Jointly modeling the numerous tracers of the disk warp at various ages and Galactic radii is the next step in uncovering the distribution of dark matter in the Galaxy.

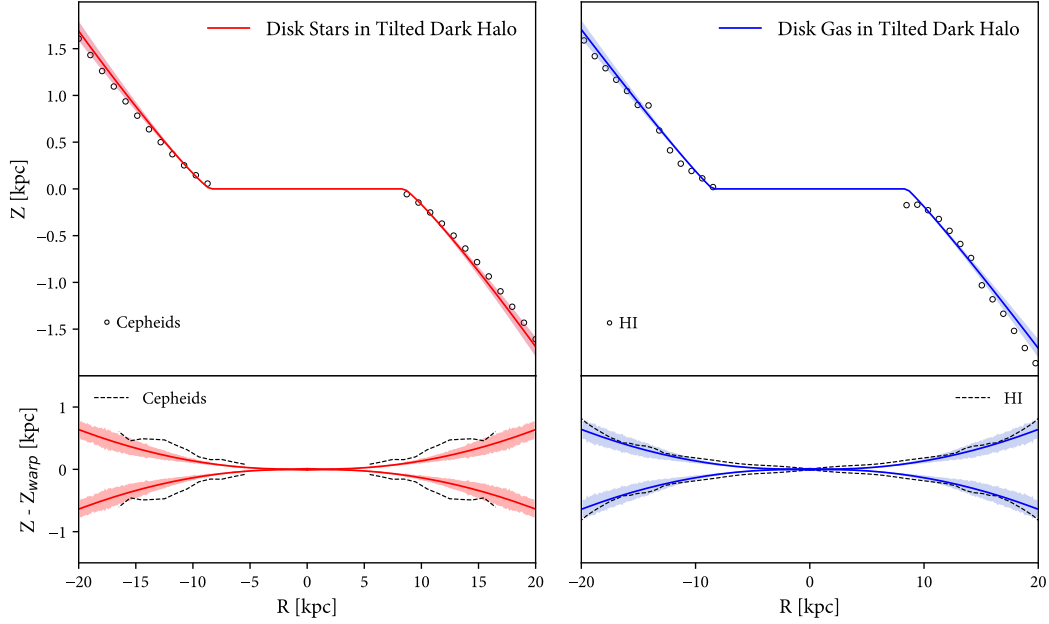


Figure 2: Comparison of the simulation to the observed warp and flare. The top panels show the warp, and bottom panels show the flare. The observed points (open circle) are extracted directly from the cited papers^{1,3,4}. (a) In the top panel, the observed warp of Cepheids¹ is plotted in open circles, and the maximum-likelihood fit of stellar warp in the simulation is plotted in red. We fix the onset radius of the warp to the observed value. Shaded regions indicate 1σ uncertainty of the fit. In the bottom panel, the observed scale height of Cepheids are plotted in black dashed lines, and the scale height of the simulated stars are plotted in red. (b) In the top panel, the observed warp of HI^{3,4} is plotted in open circles, and the maximum-likelihood fit of the gaseous warp in the simulation is plotted in blue. In the bottom panel, the observed scale height of HI is plotted in black dashed lines, and the scale height of the simulated gas are plotted in blue.

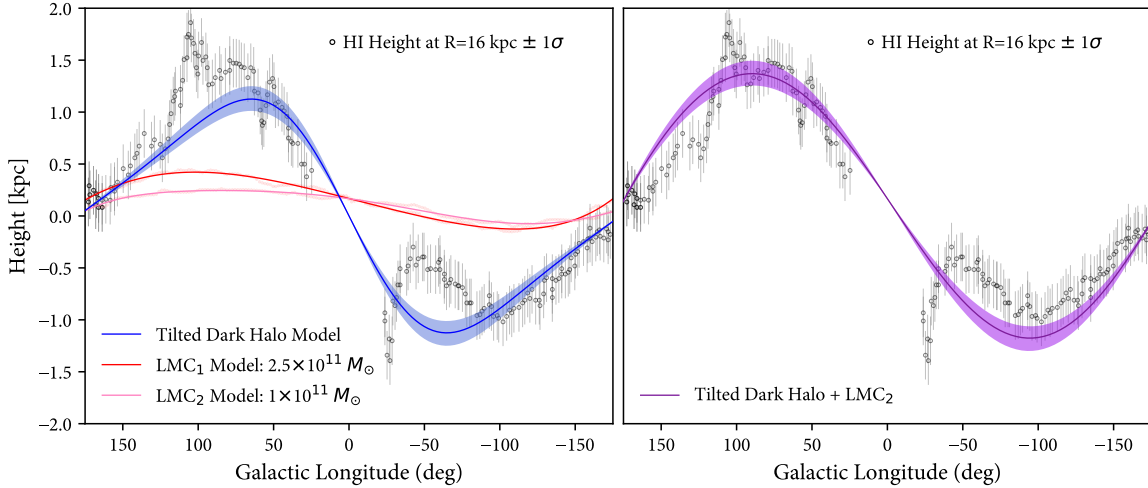


Figure 3: The amplitude and orientation of the disk warp at $R = 16$ kpc. In the left panel we plot the simulated warp from the tilted dark halo in blue, the LMC models²⁹ in red, and the HI warp in open circles³. Shaded regions indicate 1σ uncertainty of the fit. The individual data points from the LMC simulation are marked in faint dots, and a polynomial fit to the points are drawn as solid lines. In the right panel, we show the sum of the warps induced by a tilted halo and the LMC.

Methods

Simulation details

Here we describe the time-dependent Galactic potential in which we compute the orbits of tracer particles. The potential is a summation of the following components. The halo has a total mass of $8 \times 10^{11} M_{\odot}$, 70% of which is in a spherical halo with NFW⁴⁶ radial profile with scale radius $r_s = 15$ kpc, and 30% of which is in a tilted, triaxial halo. The triaxiality is 10:8.1:7.3¹⁵ and the tilt angle is 25° ¹⁵. The radial density along the principal axes of the triaxial halo follows an NFW profile with scale radius $r_s = 30$ kpc³⁵. The disk has two components: a “thick” disk with fixed mass at $6 \times 10^9 M_{\odot}$, scale radius 2 kpc, and scale height 0.9 kpc⁴⁷, and a “thin” disk that linearly increases in mass up to $3.5 \times 10^{10} M_{\odot}$ at present day, with fixed scale radius 2.6 kpc and scale height 0.3 kpc⁴⁷ assuming a Miyamoto-Nagai potential⁴⁸. The initial mass of the thin disk is $1.3 \times 10^{10} M_{\odot}$. Lastly, we include a spherical bulge with Hernquist radial profile⁴⁹ and fixed mass $1.8 \times 10^{10} M_{\odot}$ and scale radius of 1 kpc.

The tracer particles are initialized on circular orbits at radii sampled from a truncated exponential distribution, discarding any stars sampled within 1 kpc or beyond eight times the scale radius from the Galactic center. The scale radius increases linearly with time to 8 kpc at present day. The final scale radius is chosen to be where the H_2 mass surface density¹⁶ is $1/e$ of the maximum value. At each time step of the simulation, we spawn new tracer particles at a rate that is commensurate with the growth of the disk, culminating in 50,000 star particles and 50,000 gas particles. We calculate orbits using the `gala` python package⁵⁰ using a fixed 1 Myr timestep and standard Leapfrog integrator.

While the star particles are collisionless, the gas particles are collisional and follow an inelastic scattering prescription. If a gas particle comes within 0.1 kpc of another gas particle and they have negative relative speeds, they exchange relative velocities and lose 10% of the collective kinetic energy. This method of simulating gas particles is valid when the velocity dispersion is low^{51,52}, as it is the case for circular orbits. We note that all of our disk particles remain on circular orbits throughout all 5 Gyr, with the most eccentric orbits exhibiting less than 0.1% of their angular momentum off of the Galactic Z axis. Lastly, at each timestep, we allow for a probabilistic change of radius of each particle commensurate to what is measured for the Galaxy^{53,54}.

Warp Modeling

In Figure 2 we plot a fit to the warp in the simulation using an analytical formula that is a power-law in radius and a sinusoid in azimuth:

$$\begin{aligned} Z(R \geq R_w) &= A \times (R - R_w)^b \times \sin(\phi - \phi_w) \\ Z(R < R_w) &= 0 \end{aligned}$$

Here, R and Z are Galactocentric cylindrical coordinates, A is the amplitude of the warp, b the power-law index, ϕ_w the orientation of the warp, and R_w the onset radius of the warp. This function has also been used to fit the Cepheids data¹. The fit is performed using a maximum likelihood method.

Which Stars Comprise the Warp?

In Extended Data Figure 1 we color the star particles by their birth radius. We find a clear correlation in the birth radius of the star and its final warp amplitude. We can thus understand the prominence of the warp in young stars as a result of the “inside-out” growth of the disk⁵⁵, in which the birth radius of a particle correlates inversely with age. Since young stars can be born at larger radii than old stars, they trace a cleaner and larger warp. Due to radial migration⁵⁴, old stars that are born in the inner Galaxy can also migrate outwards to eventually trace the warp. This mechanism can explain why older stars appear to have smaller warp amplitudes in observations².

Timescale of the Warp

In Extended Data Figure 2 we show the time evolution of the warp amplitude at a fixed radius $R = 16$ kpc. The error bars indicate 1σ statistical uncertainties in the warp fit. At $t = 0$, the disk is initialized to have no warp. Within the first few hundred Myr, the warp reaches its maximum amplitude. This is consistent with the rotation period of the disk at 16 kpc, which is approximately 400 Myr. Thus, this Figure shows that the disk responds to the tilted dark halo quickly, within one rotation period of the disk. The warp amplitude experiences a transient oscillatory phase until 1500 Myr, then converges to a steady state. This transient phase is likely a numerical effect, since there are not many stars out at $R = 16$ kpc at these times (the tracer particle scale length is 3 kpc at $t = 0$ and 4.5 kpc at $t = 1500$ Myr) and the warp amplitude is determined by a small number of particles.

Variations to Model Parameters

In this study, we have intentionally avoided “fitting” model parameters to the data, in order to demonstrate that no tuning is required for a tilted dark halo to reproduce the observed warp/flare. In Extended Data Figures 3 and 4 we show how changes in the model parameters can affect the warp. In the former, we vary (1) the scale length of the tilted dark halo and (2) the present-day scale-length of the tracer particles. In the latter, we vary (1) the tilt angle of the dark halo and (2) the mass fraction of the tilted component of the dark halo compared to the spherical component. Aside from the parameters being modulated, all other parameters are fixed to their values from the simulation presented in Figure 1. In each panel, we calculate the fraction of stars that are off the $Z = 0$ plane by more than 0.25 kpc, $N_{\text{warp}}/N_{\text{plane}}$. If $N_{\text{warp}}/N_{\text{plane}}$ is greater than 0.5%, we fit a warp model (dotted lines) and show the warp amplitude at 20 kpc as Z_{20} . The disk warps in all models except for the case of a non-tilted halo (last row of Extended Data Figure 4). These Figures demonstrate that warping is a general response of the disk to a tilted dark halo. Furthermore, a more complete observational picture of the Galactic warp can help constrain properties of the tilted dark matter halo, such as its mass fraction and tilt angle.

Context in Cosmological Simulations

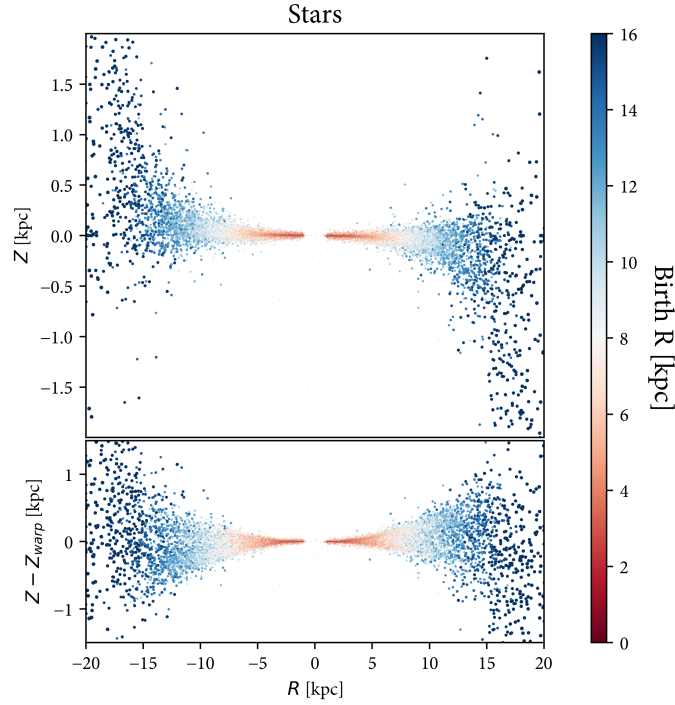
A key assumption of our idealized simulation is the fixed orientation of the halo with respect to the growing disk. It is thus important to understand to what extent these assumptions are applicable in a simulation with a live halo and self-consistently growing disk. Specifically, the time that it takes for a tilted dark halo to eventually align with the disk is an open question. If this

timescale is substantially longer than the warp onset timescale (a few hundred Myr, see Extended Data Fig. 2), then the mechanisms studied in our idealized simulation can apply more generally to slowly-changing halos.

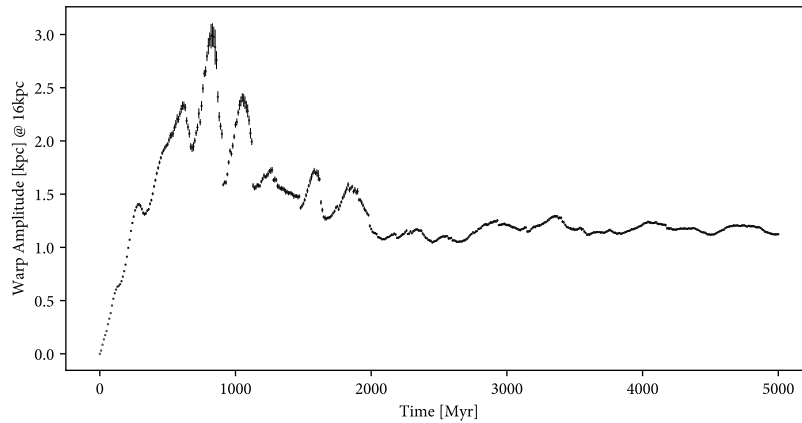
To address this question, Han et al. (in prep) analyze Milky Way-like galaxies in the Illustris TNG50 cosmological magneto-hydrodynamic simulations^{36,37}. They first show that a significant fraction of MW analogs in TNG50 have present-day tilted dark halos at $r < 50$ kpc. About 50% of halos are tilted more than 10° , and 25% of halos are tilted more than 20° . Then, they identify a galaxy that experiences a major merger at ~ 7 Gyr ago that results in a tilted dark halo. For this galaxy, the angle of misalignment of the disk and the dark halo reduces from 50° to 20° over 5 Gyr. Furthermore, the disk of this galaxy warps shortly after the onset of the tilted dark halo with a delay time of < 1 Gyr. The galaxy does not have any massive satellites at the time of the onset of the warp. TNG50 was not tuned in any way to produce these results; rather, the long-lived tilted dark halos and warps emerge naturally in the simulations. These results show that tilted dark halos can (1) be long-lived in a live, cosmological environment, and (2) generate warps in galactic disks on timescales shorter than the change in the tilt angle. Furthermore, this result shows that the Milky Way's dark halo was likely more tilted in the past and has decreased to its current value ($\sim 25^\circ$) at present day.

1. Chen, X. *et al.* An intuitive 3D map of the Galactic warp's precession traced by classical Cepheids. *Nature Astronomy* **3**, 320–325 (2019). 1902.00998.
2. Wang, H. F. *et al.* Mapping the Galactic Disk with the LAMOST and Gaia Red Clump Sample. VI. Evidence for the Long-lived Nonsteady Warp of Nongravitational Scenarios. *Astrophys. J.* **897**, 119 (2020).
3. Levine, E. S., Blitz, L. & Heiles, C. The Vertical Structure of the Outer Milky Way H I Disk. *Astrophys. J.* **643**, 881–896 (2006). astro-ph/0601697.
4. Kalberla, P. M. W., Dedes, L., Kerp, J. & Haud, U. Dark matter in the Milky Way. II. The HI gas distribution as a tracer of the gravitational potential. *Astron. Astrophys.* **469**, 511–527 (2007). 0704.3925.
5. Dame, T. M. & Thaddeus, P. A Molecular Spiral Arm in the Far Outer Galaxy. *Astrophys. J. Lett.* **734**, L24 (2011).
6. Wouterloot, J. G. A., Brand, J., Burton, W. B. & Kwee, K. K. IRAS sources beyond the solar circle. II. Distribution in the galactic warp. *Astron. Astrophys.* **230**, 21–36 (1990).
7. Drimmel, R. & Spergel, D. N. Three-dimensional Structure of the Milky Way Disk: The Distribution of Stars and Dust beyond $0.35 R_{\text{solar}}$. *Astrophys. J.* **556**, 181–202 (2001).
8. Djorgovski, S. & Sosin, C. The Warp of the Galactic Stellar Disk Detected in IRAS Source Counts. *Astrophys. J. Lett.* **341**, L13 (1989).
9. Yusifov, I. Pulsars and the Warp of the Galaxy. In Uyaniker, B., Reich, W. & Wielebinski, R. (eds.) *The Magnetized Interstellar Medium*, 165–169 (2004). astro-ph/0405517.
10. Momany, Y. *et al.* Outer structure of the Galactic warp and flare: explaining the Canis Major over-density. *Astron. Astrophys.* **451**, 515–538 (2006).
11. Cantat-Gaudin, T. *et al.* Painting a portrait of the Galactic disc with its stellar clusters. *Astron. Astrophys.* **640**, A1 (2020). 2004.07274.
12. Newberg, H. J. *et al.* The Ghost of Sagittarius and Lumps in the Halo of the Milky Way. *Astrophys. J.* **569**, 245–274 (2002). astro-ph/0111095.
13. Martin, N. F. *et al.* A dwarf galaxy remnant in Canis Major: the fossil of an in-plane accretion on to the Milky Way. *Mon. Not. R. Astron. Soc.* **348**, 12–23 (2004). astro-ph/0311010.
14. Naidu, R. P. *et al.* Evidence from the H3 Survey That the Stellar Halo Is Entirely Comprised of Substructure. *Astrophys. J.* **901**, 48 (2020). 2006.08625.
15. Han, J. J. *et al.* The Stellar Halo of the Galaxy is Tilted and Doubly Broken. *Astron. J.* **164**, 249 (2022).
16. Heyer, M. & Dame, T. M. Molecular Clouds in the Milky Way. *Annu. Rev. Astron. Astrophys.* **53**, 583–629 (2015).
17. Burke, B. F. Systematic distortion of the outer regions of the galaxy. *Astron. J.* **62**, 90 (1957).
18. Kerr, F. J., Hindman, J. V. & Carpenter, M. S. The Large-Scale Structure Of the Galaxy. *Nature* **180**, 677–679 (1957).
19. Hunter, C. & Toomre, A. Dynamics of the Bending of the Galaxy. *Astrophys. J.* **155**, 747 (1969).
20. Toomre, A. Theories of WARPS. In Athanassoula, E. (ed.) *Internal Kinematics and Dynamics of Galaxies*, vol. 100, 177–185 (1983).
21. Olling, R. P. & Merrifield, M. R. The Shape of the Milky Way's Dark Halo. In Zaritsky, D. (ed.) *Galactic Halos*, vol. 136 of *Astronomical Society of the Pacific Conference Series*, 219 (1998). astro-ph/9710224.
22. Olling, R. P. & Merrifield, M. R. Two measures of the shape of the dark halo of the Milky Way. *Mon. Not. R. Astron. Soc.* **311**, 361–369 (2000). astro-ph/9907353.
23. Sparke, L. S. & Casertano, S. A model for persistent galactic warps. *Mon. Not. R. Astron. Soc.* **234**, 873–898 (1988).
24. Debattista, V. P. & Sellwood, J. A. Warped Galaxies from Misaligned Angular Momenta. *Astrophys. J. Lett.* **513**, L107–L110 (1999). astro-ph/9901153.
25. Jiang, I.-G. & Binney, J. WARPS and cosmic infall. *Mon. Not. R. Astron. Soc.* **303**, L7–L10 (1999). astro-ph/9807161.
26. Poggio, E. *et al.* Measuring the vertical response of the Galactic disc to an infalling satellite. *Mon. Not. R. Astron. Soc.* **508**, 541–559 (2021). 2011.11642.
27. Ostriker, E. C. & Binney, J. J. Warped and tilted galactic discs. *Mon. Not. R. Astron. Soc.* **237**, 785–798 (1989).
28. Dubinski, J. & Chakrabarty, D. Warps and Bars from the External Tidal Torques of Tumbling Dark Halos. *Astrophys. J.* **703**, 2068–2081 (2009).
29. Laporte, C. F. P., Gómez, F. A., Besla, G., Johnston, K. V. & Garavito-Camargo, N. Response of the Milky Way's disc to the Large Magellanic Cloud in a first infall scenario. *Mon. Not. R. Astron. Soc.* **473**, 1218–1230 (2018).
30. Erkal, D. *et al.* The total mass of the Large Magellanic Cloud from its perturbation on the Orphan stream. *Mon. Not. R. Astron. Soc.* **487**, 2685–2700 (2019). 1812.08192.
31. Prada, J., Forero-Romero, J. E., Grand, R. J. J., Pakmor, R. & Springel, V. Dark matter halo shapes in the Auriga simulations. *Mon. Not. R. Astron. Soc.* **490**, 4877–4888 (2019).
32. Emami, R. *et al.* Morphological Types of DM Halos in Milky Way-like Galaxies in the TNG50 Simulation: Simple, Twisted, or Stretched. *Astrophys. J.* **913**, 36 (2021).
33. Debattista, V. P. *et al.* What's up in the Milky Way? The orientation of the disc relative to the triaxial halo. *Mon. Not. R. Astron. Soc.* **434**, 2971–2981 (2013). 1301.2670.
34. Shao, S., Cautun, M., Deason, A. & Frenk, C. S. The twisted dark matter halo of the Milky Way. *Mon. Not. R. Astron. Soc.* **504**, 6033–6048 (2021). 2005.03025.
35. Han, J. J. *et al.* A Tilt in the Dark Matter Halo of the Galaxy. *Astrophys. J.* **934**, 14 (2022).
36. Pillepich, A. *et al.* First results from the TNG50 simulation: the evolution of stellar and gaseous discs across cosmic time. *Mon. Not. R. Astron. Soc.* **490**, 3196–3233 (2019). 1902.05553.
37. Nelson, D. *et al.* The IllustrisTNG simulations: public data release. *Computational Astrophysics and Cosmology* **6**, 2 (2019). 1812.05609.
38. Belokurov, V., Erkal, D., Evans, N. W., Koposov, S. E. & Deason, A. J. Co-formation of the disc and the stellar halo. *Mon. Not. R. Astron. Soc.* **478**, 611–619 (2018). 1802.03414.

39. Helmi, A. *et al.* The merger that led to the formation of the Milky Way's inner stellar halo and thick disk. *Nature* **563**, 85–88 (2018). 1806.06038.
40. Gallart, C. *et al.* Uncovering the birth of the Milky Way through accurate stellar ages with Gaia. *Nature Astronomy* **3**, 932–939 (2019). 1901.02900.
41. Bonaca, A. *et al.* Timing the Early Assembly of the Milky Way with the H3 Survey. *Astrophys. J. Lett.* **897**, L18 (2020). 2004.11384.
42. Naidu, R. P. *et al.* Reconstructing the Last Major Merger of the Milky Way with the H3 Survey. *Astrophys. J.* **923**, 92 (2021). 2103.03251.
43. Lilleengen, S. *et al.* The effect of the deforming dark matter haloes of the Milky Way and the Large Magellanic Cloud on the Orphan-Chenab stream. *Mon. Not. R. Astron. Soc.* **518**, 774–790 (2023).
44. Peter, A. H. G., Rocha, M., Bullock, J. S. & Kaplinghat, M. Cosmological simulations with self-interacting dark matter - II. Halo shapes versus observations. *Mon. Not. R. Astron. Soc.* **430**, 105–120 (2013). 1208.3026.
45. Evans, N. W., O'Hare, C. A. J. & McCabe, C. Refinement of the standard halo model for dark matter searches in light of the Gaia Sausage. *Phys. Rev. D* **99**, 023012 (2019).
46. Navarro, J. F., Frenk, C. S. & White, S. D. M. A Universal Density Profile from Hierarchical Clustering. *Astrophys. J.* **490**, 493–508 (1997). astro-ph/9611107.
47. Bland-Hawthorn, J. & Gerhard, O. The Galaxy in Context: Structural, Kinematic, and Integrated Properties. *Annu. Rev. Astron. Astrophys.* **54**, 529–596 (2016). 1602.07702.
48. Miyamoto, M. & Nagai, R. Three-dimensional models for the distribution of mass in galaxies. *Publications of the Astronomical Society of Japan* **27**, 533–543 (1975).
49. Hernquist, L. An Analytical Model for Spherical Galaxies and Bulges. *Astrophys. J.* **356**, 359 (1990).
50. Price-Whelan, A. M. Gala: A Python package for galactic dynamics. *The Journal of Open Source Software* **2**, 388 (2017).
51. Negroponte, J. & White, S. D. M. Simulations of mergers between disc-halo galaxies. *Mon. Not. R. Astron. Soc.* **205**, 1009–1029 (1983).
52. Carlberg, R. G. & Freedman, W. L. Dissipative models of spiral galaxies. *Astrophys. J.* **298**, 486–492 (1985).
53. Frankel, N., Rix, H.-W., Ting, Y.-S., Ness, M. & Hogg, D. W. Measuring Radial Orbit Migration in the Galactic Disk. *Astrophys. J.* **865**, 96 (2018). 1805.09198.
54. Sellwood, J. A. & Binney, J. J. Radial mixing in galactic discs. *Mon. Not. R. Astron. Soc.* **336**, 785–796 (2002). astro-ph/0203510.
55. Frankel, N., Sanders, J., Rix, H.-W., Ting, Y.-S. & Ness, M. The Inside-out Growth of the Galactic Disk. *Astrophys. J.* **884**, 99 (2019). 1909.07118.

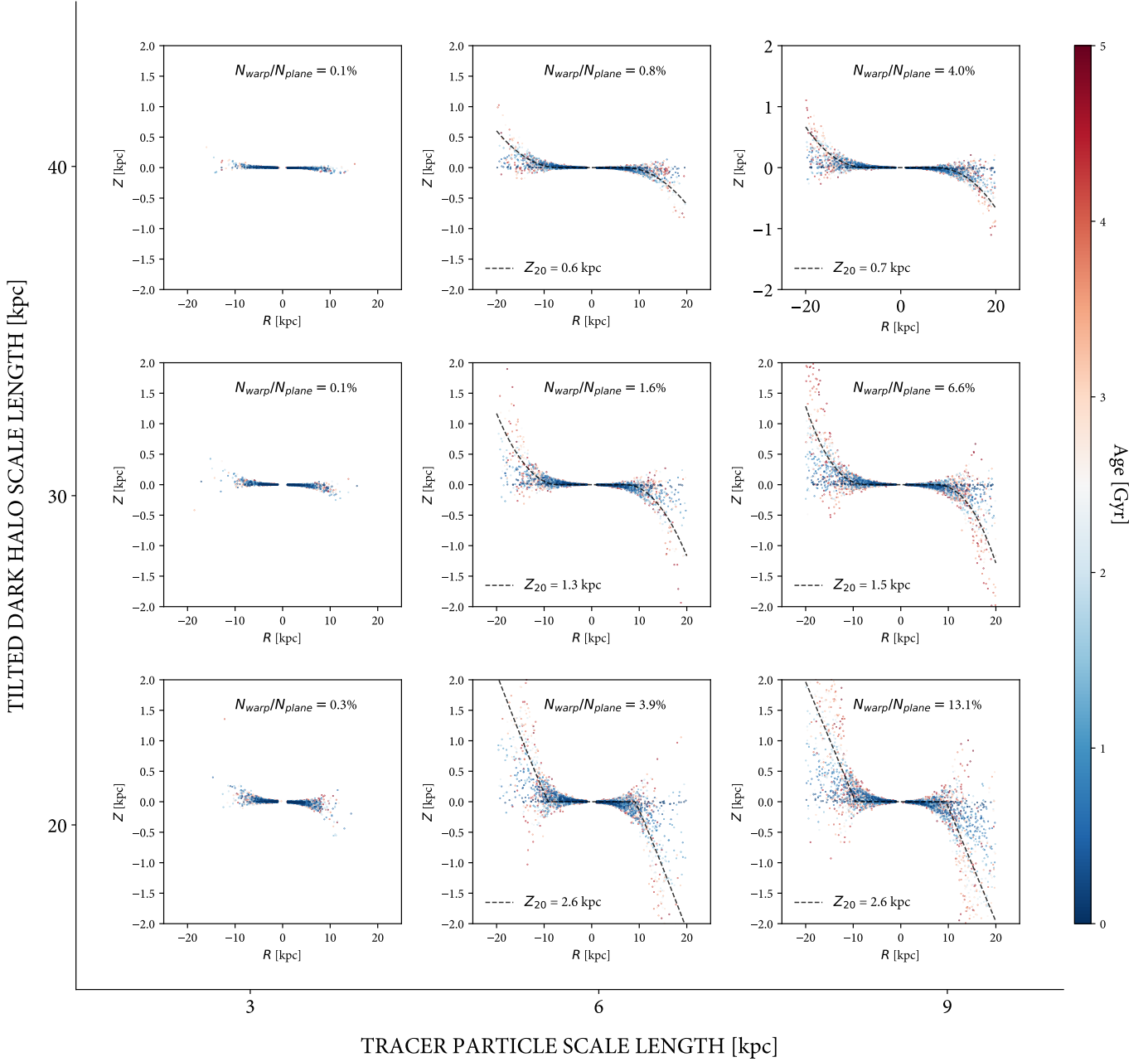


Extended Data Fig. 1: Present-day distribution of star particles in the simulation in Galactocentric cylindrical coordinates. Negative R indicates azimuthal angles that are within 90° of the Northern warp, and positive R indicates azimuthal angles that are within 90° of the Southern warp. The top panels show the warp, and the bottom panels show the vertical deviation from the average warp. The vertical deviation systematically increases toward the outer Galaxy, demonstrating the flare of the disk. Points that are in the outer Galaxy are plotted with larger circles. Particles colored by birth radius reveal that the magnitude of the warp correlates strongly with the birth radius.



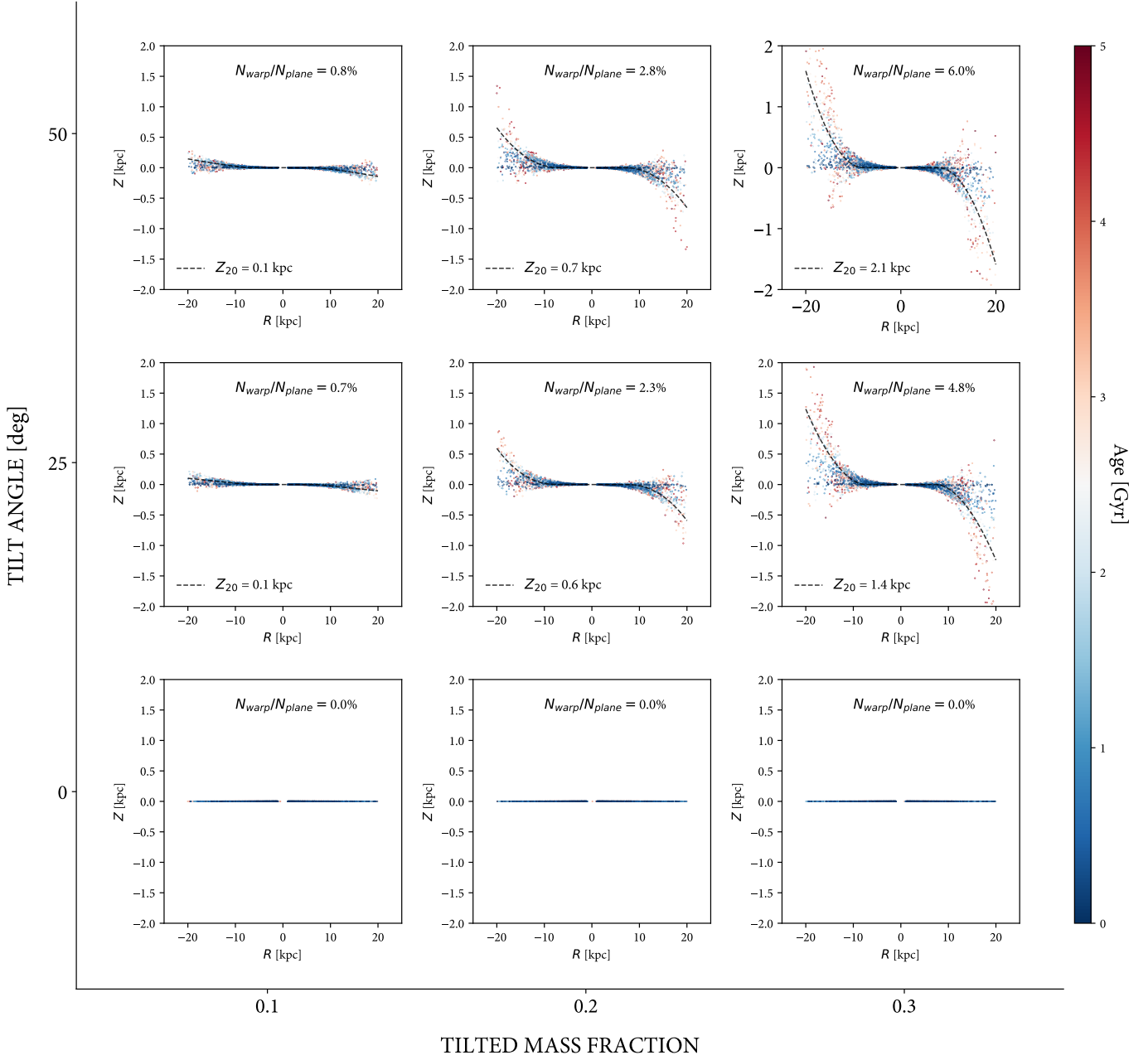
Extended Data Fig. 2: Time evolution of the warp amplitude at fixed radius $R = 16$ kpc. At $t = 0$, the disk is initialized to have no warp. Error bars indicate 1σ statistical uncertainty in the warp fit. Within a few hundred Myr, the warp reaches maximum amplitude. After a transient oscillatory phase from $t = 500 - 1500$ Myr, the warp reaches a steady-state amplitude. This plot demonstrates that the warp onsets quickly, within one rotation period of the disk (400 Myr for a star at 16 kpc).

Variation of Model Parameters



Extended Data Fig. 3: Variation of (1) the scale length of the tilted component of the dark halo and (2) the present-day scale length of the tracer particles. Aside from the two parameters being modulated, all other parameters are fixed to the simulation presented in Figure 1. In each panel, we show the fraction of stars that are off the $Z = 0$ plane by more than 0.25 kpc, N_{warp}/N_{plane} . If this fraction is greater than 0.5%, we fit a warp model (dotted lines) and show the warp amplitude at 20 kpc as Z_{20} . The warp amplitude correlates positively with the scale length of the disk, and anti-correlates with the scale length of the tilted dark halo.

Variation of Model Parameters



Extended Data Fig. 4: Variation of (1) the tilt angle of the dark halo (2) the mass fraction of the tilted component of the dark halo. Aside from the two parameters being modulated, all other parameters are fixed to the simulation presented in Figure 1. Similar to Extended Data Figure 3, we show the fraction of stars that are off the $Z = 0$ plane by more than 0.25 kpc, N_{warp}/N_{plane} . If this fraction is greater than 0.5%, we fit a warp model (dotted lines) and show the warp amplitude at 20 kpc as Z_{20} . The warp amplitude correlates positively with both the tilt angle and the mass fraction of the tilted halo.